TUDelft

Delft University of Technology

The effects of wave non-linearity on wave attenuation by vegetation

Phan, K. L.; Stive, M. J.F.; Zijlema, M.; Truong, H. S.; Aarninkhof, S. G.J.

Important note
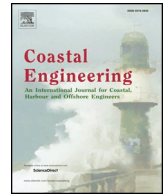To cite this publication, please use the final published version (if applicable).
Please check the document version above.

The effects of wave non-linearity on wave attenuation by vegetation

K.L. Phan[a,b], M.J.F. Stive[a,*], M. Zijlema[a], H.S. Truong[a,b], S.G.J. Aarninkhof[a]

[a] Hydraulic Department, Faculty of Civil Engineering and Geosciences, Delft University of Technology, the Netherlands
[b] Hydraulic Department, Faculty of Civil Engineering, Thuy Loi University, Vietnam

ABSTRACT

Wave attenuation through mangrove forests has received more and more attention, especially in the context of increasing coastal erosion and sea-level-rise. Numerous studies have focused on studying the reduction of wave height in a mangrove forest. However, the understanding of this attenuation process is still in its infancy. In order to obtain more insight, a laboratory experiment, mimicking the processes of wave attenuation by coastal mangroves in the Mekong Delta, Vietnam was conducted. The reduction of wave height for different scenarios of mangrove densities and wave conditions was investigated. A new method to quantify vegetation attenuation induced by vegetation is presented. The wave height reduction is presented over a relative length scale (viz. the number of wavelengths), instead of an absolute length scale of the forest (e.g per meter or per 100 m). The effects of wave non-linearity on the wave height attenuation over the mangrove forest were investigated using the Ursell number. It is suggested that the non-linear character of waves has a strong influence on the attenuation of the waves inside the mangrove forest. A numerical model, mimicking the experiment was constructed in SWASH and validated using the experimental data. Finally, the data set was extended through numerical modelling so that a larger ranging relationship between wave attenuation per wave length and the Ursell number could be formulated.

1. Introduction

In recent decades, many coastal and estuarine regions around the world have been recorded to suffer from accelerated erosion due to the effects of global warming, sea-level-rise and subsidence. In this context, the defensive role of ecosystems in general and mangrove forests in particular for coastal areas has been increasingly recognized. The complex system of roots, stems and canopies enables mangroves to absorb external forces such as due to waves and currents.

Understanding the mechanism of wave height reduction by mangroves is an important step in understanding the hydrodynamic, sedimentation and exchange processes in mangrove forests. Numerous studies have been published focusing on this topic (Mazda et al., 1997; Mazda et al., 2006; Massel, 2006; Quartel et al., 2007; Bao, 2011; Brinkman et al., 1997; Brinkman, 2006; Augustin et al., 2009). It is accepted that waves travelling through a mangrove forest perform work on vegetation roots, stems and canopies, thereby losing their energy and reducing their wave height (Dalrymple et al., 1984; Mork, 1996).

The reduction of wave height depends on the vegetation characteristics *i.e.* the density, stiffness etc. and the wave characteristics *i.e.* at least the wave height and wave period (Mendez and Losada, 2004). However, the effect of the wave characteristics on the wave height reduction through a mangrove forest is less clarified than that of the cylinder density. While Bradley and Houser (2009) suggested that the wave attenuation through the vegetation reduces with increasing wave height, Cavallaro et al. (2011) observed more wave height reduction when the wave height increases.

Anderson and Smith (2015), based on a laboratory study of irregular wave dissipation through submerged and emerged flexible vegetation, suggested that the wave attenuation appears to strongly depend on the ratio of stem length to water depth and stem density. Additionally, it is shown that under emergent conditions the high frequency waves attenuated more than the low-frequency waves. These results are in line with the results of Phan et al. (2014).

The effect of wave characteristics in general and wave non-linearity in particular on the attenuation rate of wave height due to the emerged and rigid vegetation is not fully understood. As a result, although many physical models have been conducted, combined with calibration or validation of advanced numerical models, most studies only focus on the attenuation of regular waves, and only over a limited distance of vegetation length in the range of 1–4 m). Data sets for model validation in this context are also lacking.

Therefore, the main objectives of this study are to (1) study the role of wave characteristics on the wave attenuation processes, (2) to

provide and extend the data sets for advanced analyses and validation, using both a physical and a numerical model.

2. Methodology

In order to achieve the research objectives, physical and numerical modelling were chosen as major approaches. Their set-up and configurations are described in this section of the paper. First, a physical experiment mimicking the wave attenuation processes by mangroves in the Mekong Delta was conducted. Second, a numerical model was constructed and validated with the experimental data. The combined results were analysed to study the effects of wave characteristics and non-linearity on the wave attenuation by the vegetation.

2.1. Physical modelling

A laboratory experiment of wave attenuation through cylinder arrays, mimicking wave attenuation processes through a coastal mangrove forest was conducted in a flume of the Fluid Mechanics Laboratory at Delft University of Technology. The effective length, height and width of the flume is 40 m, 1 m and 0.8 m respectively.

Fig. 1 gives a cross-section of the experimental set up. The wave generator with an active wave absorption system was placed at the beginning of the flume to prevent reflected waves from reflecting again into the flume. The 2nd order wave steering was always active during the experiment.

Because the Mekong Delta coast has generally a very gentle slope of about 1/10000, waves propagating towards the mangroves are usually broken before entering the mangrove forests (Phan et al., 2014). As a result, they have lost their primary spectral energy and long wave energy has developed. Therefore a steep wooden slope with a combination slope of 1/10 and 1/20 was used to simulate the processes of shoaling and breaking waves. This situation was considered in the experiments named broken wave scenarios. In addition to that, there are also situations where waves are not broken such as waves generated by strong local wind. This circumstance also was considered in the experiment regarding the so named non-broken wave scenarios. It is noticed that the broken or non-broken wave conditions described in this study represent the wave modes before entering the mangrove forest. It is observed that wave breaking processes did virtually not occur inside the mangrove forests in all experimental scenarios.

Over a length of 17.5 m cylinder arrays were installed along a horizontal bottom. The wave height and the depth-averaged velocity were measured by 13 wave gauges and seven electromagnetic velocity meters (EMS) with a sampling rate of 100 Hz. Representative locations of the equipment are indicated in Fig. 1. The experiments were repeated with different locations of the equipment to obtain more data inside the vegetation. Wave height and velocity measurements were taken over a long time interval so at least 100 waves in scenarios of regular waves and 1000 waves in scenarios of irregular waves so that representative statistical data could be achieved. Typical values in the experiment are: a water depth in front of the wave paddle of 65 cm; wave heights
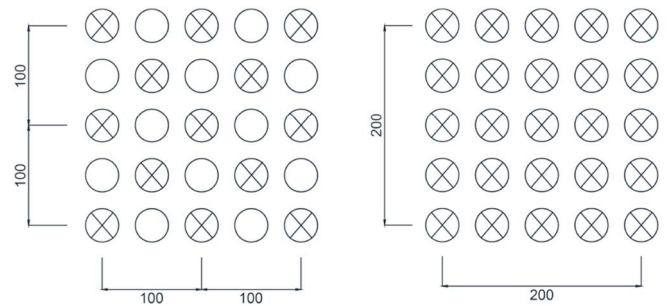

Fig. 2. Cylinder distribution used in the experiment (unit in mm). Not to scale.

ranging from 1 to 10 cm; and wave periods ranging from 1 to 3s. In most experiments, a wave absorber was placed at the end of the flume to reduce wave reflections. Some additional experiments were done with a wooden sea-dike at the end with slope 1:5, representing the sea-dikes usually constructed right behind the mangrove forests along the Mekong Delta coast (Phan et al., 2014).

Fig. 2 shows the arrangements of the cylinder arrays which were considered in the experiment. The density of the cylinder arrays was based on the solid volume fraction of the mangrove forest. The solid volume fraction per unit volume can be calculated according to: $V_s = N \frac{\pi d^2}{4}$ where d is the diameter of the cylinder: d = 0.012 m and N is the density of mangroves. In this way, there are 2 densities of mangroves considered, which are 200 cylinders/m^2 (sparse cases) and 400 cylinders/m^2 (dense cases), yielding V_s values of 2% and 4% respectively.

Based on the set up described above, the experiments were performed for different cases of wave heights and wave periods, including regular and irregular, non-broken waves (Type 1) and broken waves (Type 2). Further details are given in Table 1.

2.2. Numerical model

A numerical model mimicking the experiment was constructed based on the SWASH model. The SWASH model is a time domain model for simulating non-hydrostatic, free surface, rotational flows, in which the governing equations of the model are the shallow water equations including a non-hydrostatic pressure term (Zijlema, Stelling & Smit, 2011b). The presence of vegetation in SWASH was modelled through Morrison's equation:

$$F_x = \frac{1}{2}\rho C_D h_v b_v N_v u|u| \tag{1}$$

in which ρ is gravitational acceleration, C_D is a bulk drag coefficient, h_v is the height of the cylinder, b_v is the diameter of the cylinder. N_v is the number of plants per square meter and u is the horizontal velocity due to wave motion.

The numerical model was constructed based on the physical model in such a way that the numerical results can be directly compared with the experimental results. Specific settings described below are related
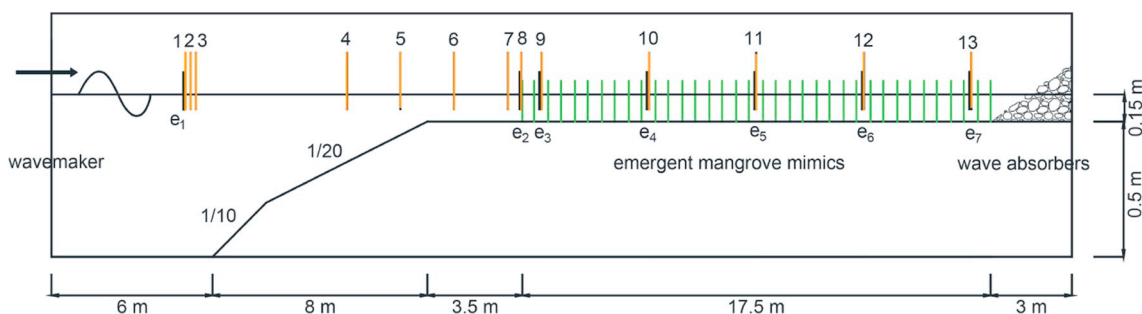

Fig. 1. Schematic view of the experiment set up, including the locations of wave gauges, EMSs and vegetation. Not to scale.

Table 1
Experimental scenarios.

Vegetation	Wave characteristics	Regular (Re)		Irregular (Ir)	
		H (cm)	T(s)	Hs (cm)	Tp (s)
without mangroves	Broken (Type 2)	10	2.0; 2.5; 3.0	10	2.0; 2.5; 3.0
with mangroves	Non-broken (Type 1)	1; 2; 3; 4; 5	2.0; 2.5; 3.0	3; 5	2.0; 2.5; 3.0
	Broken (Type 2)	7; 10	2.0; 2.5; 3.0	7; 9; 10; 13; 15	2.0; 2.5; 3.0

to boundary conditions and vegetation properties. The minimum grid size is 0.01 m. This results in about 4000 active grid points. This means that there is about 50–100 grid cells per wavelength. The time step was chosen as small as 0.001s. The hydraulic boundary conditions of the numerical model were prescribed based on the experimental configurations. At the end of the model, three different types of constructions were applied which are (1) a sponge layer in which there is no wave reflection, (2) a permeable slope corresponding to the cases with wave absorber (stone size 0.03 m and (porosity 40%) and (3) an impermeable slope representing the case with a sea dike at the end of the flume (slope 1/5).

The predictive skill of SWASH was calculated using the bias and the scatter index SI, which are given by:

$$bias = \frac{1}{N} \sum_{i=1}^{N} \left(\varphi_{comp}^i - \varphi_{obs}^i \right) \tag{2}$$

and

$$SI = \frac{\sqrt{\frac{1}{N} \sum_{i=1}^{N} \left(\varphi_{comp}^i - \varphi_{obs}^i \right)^2}}{\frac{1}{N} \sum_{i=1}^{N} \varphi_{obs}^i} \tag{3}$$

In which, N is the total number of data points in a given data set, φ_{comp} is the wave parameter computed by SWASH and φ_{obs} is the corresponding observed wave parameter (Zijlema, 2012). The simulation time in cases of irregular waves is 60 m and in cases with regular waves 20 m.

3. Experimental results

In this section, wave attenuation is evaluated using wave transmission coefficients, *i.e.* according to the number of wavelengths. The relationship between wave non-linearity and wave attenuation is examined using the Ursell number, which is an indicator of wave non-linearity.

3.1. Wave attenuation per unit distance of the mangrove forest

In the literature, the reduction of wave heights inside the vegetation is usually presented through the wave transmission coefficient (K_t). It is the ratio between the transmitted wave height (H_x) and the wave height at the starting location of the mangroves (H_0 at $x = 0$ m). H_x is the root mean squared wave height at location x inside the mangrove forest.

$$K_t = \frac{H_x}{H_o} \tag{4}$$

The impacts of vegetation on the transformation processes can be revealed by comparing this wave transmission coefficient along the forest in cases of different vegetation densities (no vegetation: $N = 0$; sparse: $N = 200$ cylinders/m^2 and dense: $N = 400$ cylinders/m^2). Fig. 3 shows the wave transmission coefficient (Kt) along the mangrove forest in cases of 10 cm wave height at the wave paddle with different wave periods (Tp = 2.0; 2.5 and 3 s), wave conditions (regular and irregular), and with different mangrove densities (no mangroves, sparse and dense).

In scenarios without vegetation, it can be seen that the wave transmission coefficient remains almost the same along the bare horizontal bottom. The wave height is slightly reduced probably due to bottom friction. Moreover, there is a fluctuation of K_t along the flume. Waves reflected from the end of the flume are the possible reason for this fluctuation. However, this phenomenon is not observed in cases with vegetation. K_t does not fluctuate but continuously reduces toward the end of the forest. This means that the reflected waves in the flume are also damped. This result reveals the capability of vegetation in reducing not only the incoming waves but also the wave reflection from the sea dike.

In scenarios with sparse vegetation, the wave height was damped about 60 percent after passing through 17.5 m length of mangroves. In scenarios with dense cylinder arrays, around 70 percent of the wave height was damped at the end of the forest. In this sense, the denser the vegetation, the smaller the wave transmission coefficient Kt and vice versa. It is noted that although the density of mangroves was doubled from 200 stems/m^2 to 400 stems/m^2 (V_s increases from 2% to 4%), the attenuation wave increased only 10 percent. In this context, 1% of V_s appears to corresponds to about 5% of wave height reduction, which means that if the solid volume fraction (V_s) increases to 20%, the wave height could be nearly total damping.

3.2. Wave attenuation per wave length

In the above section of this paper, the result of wave height reduction in the experiment is examined through the wave transmission coefficient K_t. In the literature, it is noticed that the evaluation of the wave attenuation according to K_t appears to be not consistent. For example, the wave attenuation was calculated per 100 m (Mazda et al., 1997), per 1 m (Mazda et al., 2006; Massel, 2006; Quartel et al., 2007; Bao, 2011; Möller et al., 1999; Möller and Spencer, 2002; Möller, 2006; Cooper, 2005; Bradley and Houser, 2009; Lövstedt and Larson, 2009) or per length of the forest (Brinkman et al., 1997; Brinkman, 2006). As a result, the rate of wave attenuation in the literature is hardly informative.

Moreover, one should bear in mind that the attenuation of waves by mangroves does not only depend on vegetation characteristics such as diameter, density and distribution of roots, stems and canopies, but also on the characteristics of incoming wave groups *i.e* broken and non-broken, long and short, large and small waves. Therefore, in order to include more physics in studying the wave attenuation processes, the reduction of waves is presented over a relative distance, viz the number of wavelengths instead of the length of the mangrove forest or an arbitrary absolute length. In this way, the influences of wave characteristics on the wave attenuation processes can be interpreted more easily and the observed large variation in the wave attenuation in the literature is expected to be reduced.

The total wave attenuation per meter of wavelength (K_L), or the effective wave transmission coefficient is defined as:

$$K_L = \frac{H_L}{H_o} \tag{5}$$

where H_L is the root mean squared wave height after a certain number of wavelength (n) and H_o is the root mean squared wave height at the mangrove edge ($n = 0$).
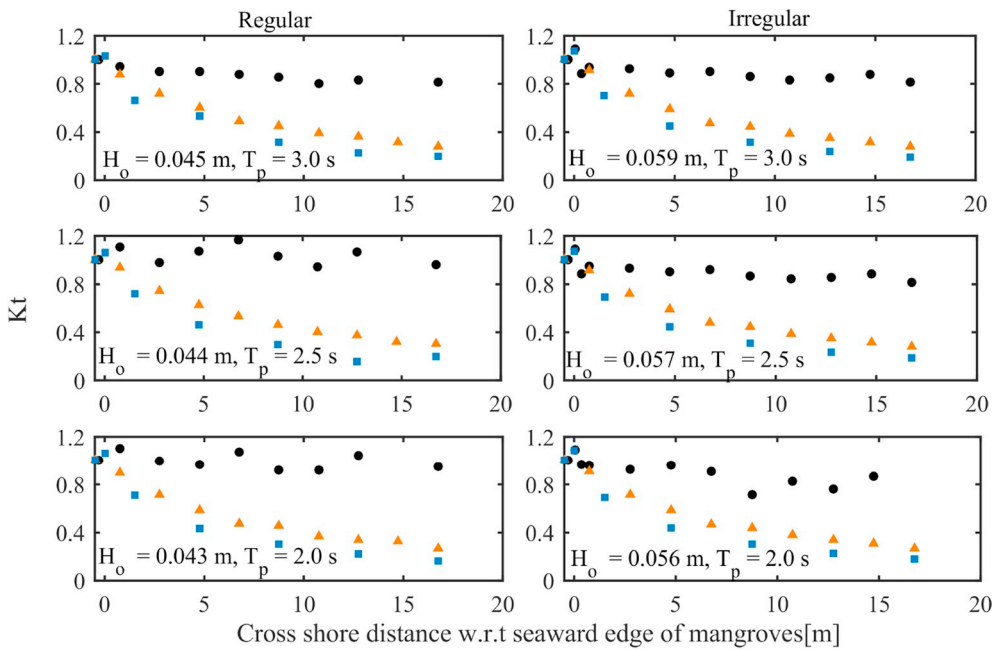
Fig. 3. Wave transmission coefficient Kt in cases of different mangroves densities: no mangroves (circles), V1 = 200 units/m2 (triangles) and V2 = 400 units/m2 (squares). A wave height of 10 cm, with different wave periods of 3.0s (upper panels); 2.5s (middle panels) and 2.0s (lower panels). Left-hand side: regular waves. Right-hand side: irregular waves. H_0 is the wave height measured at the vegetation edge.
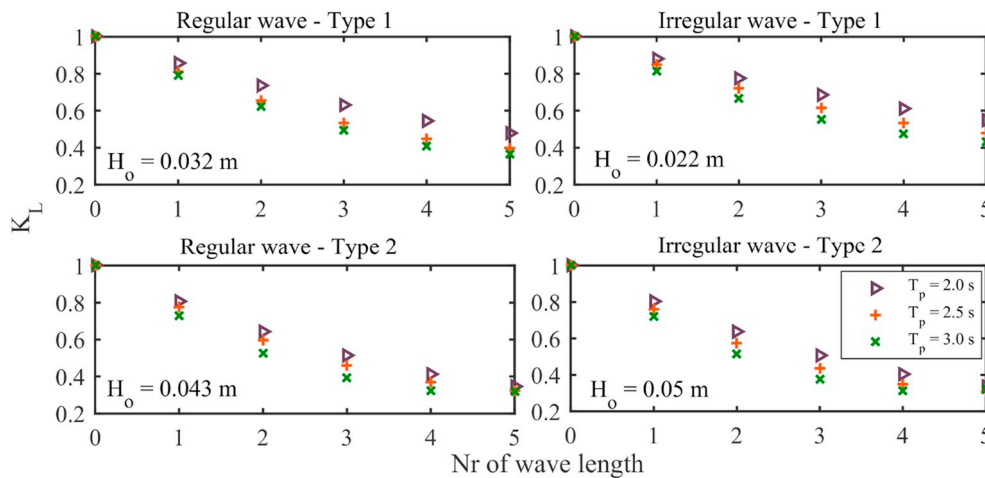

Fig. 4. Effective wave transmission K_L in cases of sparse mangroves, different wave periods: $T_p = 2$ s (black triangles), $T_p = 2.5$ s (red pluses) and $T_p = 3$ s (green crosses). (For interpretation of the references to colour in this figure legend, the reader is referred to the Web version of this article.)

Fig. 4 shows the correlation between the effective wave transmission coefficient (K_L) and the number of wavelengths in scenarios of non-broken waves (upper panels) and broken waves (lower panels) with the same wave height and different wave periods. It can be seen that the larger the number of wave lengths, the smaller the effective wave transmission coefficient (K_L). Moreover, in all considered scenarios, although the wave height was damped 15%–20% after the first wavelength, only about 40% of the wave height was damped in the next four wave lengths i.e. 8% per wavelength. In this sense, wave damping over the first wave length is the most effective. Furthermore, it can also be seen that the larger the wave period, the smaller the effective wave transmission coefficient i.e. the more wave damping.

The influence of wave height on wave attenuation was revealed by comparing the K_L in non-broken cases of the same wave period, but with different wave height, (Fig. 5). In scenarios of non-broken regular waves (upper left panel), it is suggested that the larger the wave height, the larger the wave attenuation and vice versa. In the case with 5 cm wave height at the mangrove edge (orange crosses), wave height was damped about 20% after the first wave length and more than 62% in the next four wave lengths. However, in the case of 1 cm wave height

(blue left-pointing triangles), only about 5% of the wave height is damped after the first wave length, while up to 25% of the wave height is damped after the next four wave lengths. It appears that larger waves of the same period attenuate stronger. Similar results were also observed in cases of non-broken irregular waves (upper right panel).

In scenarios of broken regular waves (lower left panel), the incoming waves have already reduced their height due to the breaking process before entering the mangrove forest. As a result, even when the wave height at the wave paddle is quite different ($H = 0.07$ m and 0.1 m), the wave height at the edge of the mangrove forest is almost the same ($H_0 = 0.043$ m and 0.044 m, respectively) which results in a similar attenuation process inside the mangrove forest. In scenarios of broken irregular waves (lower right panel), although the wave height at the wave paddle are the same as that in cases of broken regular waves ($H = 0.07$ m and 0.1 m), the wave height at the mangrove edge are slightly different ($H_0 = 0.043$ m and 0.05 m, respectively). This is due to the differences in the breaking processes between the regular and irregular waves. However, the wave attenuation processes inside the mangroves in regular and irregular cases appears to be similar.

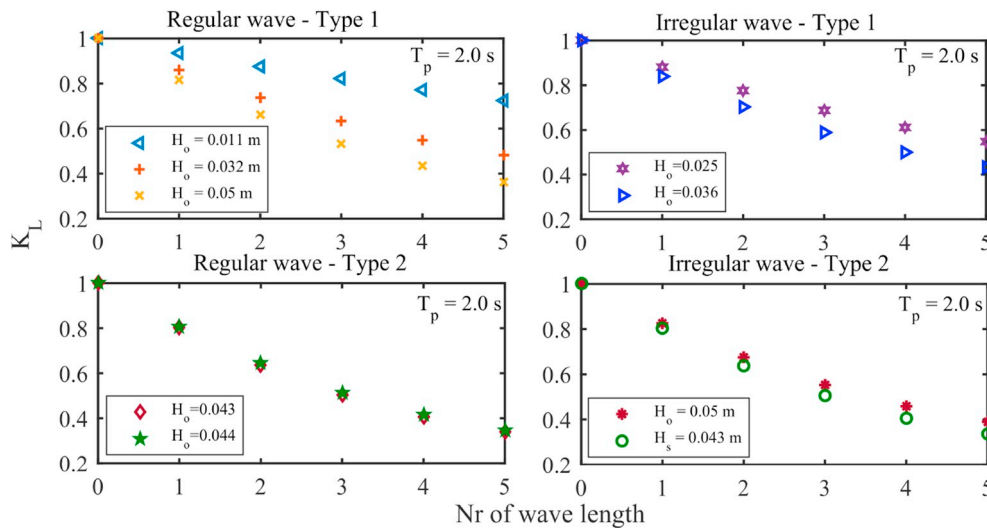Overall, by presenting the effective wave transmission coefficient,

Fig. 5. Effective wave transmission K_L in cases of sparse vegetation, wave period of 2s, different wave height.

the variation of wave attenuation rate appears to be reduced as being expected. The small scatter that remains is possibly caused by the non-linearity of the wave characteristics, which is examined in the following section.

3.3. Effect of wave non-linearity on wave attenuation by mangroves

By determining the reduction of the wave height according to a relative length scale *i.e.* wave length, it is suggested that the damping of the waves depends on the wave characteristics. In this sense, an overall indicator accounting for the wave characteristics in studying the wave attenuation processes is required. In the literature, most studies on wave height attenuation processes through the vegetation are usually simplified by adopting the four main assumptions: (1) vegetation consists of rigid plants (2) waves are regular, (3) vegetation is emerged and uniform and (4) waves follow linear theory. The effects of wave characteristic in general and wave non-linearity in particular on the attenuation processes have received less attention. In this section, the influence of wave non-linearity on the wave attenuation through a mangrove forest are examined.

The influences of wave non-linearity on the wave damping through vegetation were studied in Wu and Cox (2015). A relationship between the Ursell number (varied from 0 to 60) and the drag coefficient was shown based on an experiment of the damping of non-broken, irregular waves through an I1.8 m long stretch of cylinder arrays. It is suggested that the wave steepness influences the wave attenuation by vegetation. In this study, Ursell numbers (in the range of 20–250) were used to clarify the impact of wave non-linearity on the wave damping through mangroves for both non-broken and broken irregular wave and non-broken regular waves. The Ursell number is defined as:

$$Ursell = \frac{H_s L^2}{h^3} \qquad (6)$$

where H_s is the significant wave height (m); h is the water depth (m); and L is the wave length (m), with all parameter values at the mangrove edge.

Fig. 6 shows the relationship between the effective wave transmission coefficient and the Ursell number for a varying number of wave lengths. It can be clearly seen that as the Ursell number increases, K_L reduces implying an increase in the wave reduction. This result means that the wave dissipation by vegetation appears to be more effective as the waves are more non-linear. Moreover, as the Ursell number increases to above 150, the declination of the K_L reduces. K_L appears to achieve an equilibrium value when the Ursell number is larger than

250. This means that the wave heigh reduction no longer depends on the wave non-linearity. This characteristic can be observed for both regular and irregular waves.

It can be seen that the influence of mangrove density on the wave attenuation process is different for different numbers of wave length. For the first wave length, the difference of K_L between the sparse cases and dense cases is about 10% (upper panels in Fig. 6). However, after three wave lengths, this difference increases to about 20% (lower panels in Fig. 6). Furthermore, it is suggested that the effect of wave-nonlinearity on the wave height reduction also depends on the numbers of wave length. For instance, over the first wave length, the wave attenuation increases about 20% (K_L reduce from about 0.9 to 0.7) as the Ursell increases from 50 to 250. However, after 3 wave lengths, the wave attenuation increases about 35% when the Ursell number increases from 50 to 250. A similar trend was observed for both regular and irregular waves.

4. Numerical results

The capability of the SWASH model in the reproduction of the wave transformation in cases without vegetation has been well validated (Zijlema, Stelling & Smit, 2011a; Buckley et al., 2014; Zijlema, Stelling & Smit, 2011a), but cases with vegetation have received more attention only recently (Cao et al., 2016). Data sets presenting wave transformation over a long vegetation distance are needed. In this section, the capability of the SWASH model in the simulation of the wave transformation processes over an elongated 24 m foreshore with and without vegetation was validated using experimental results. Moreover, the model was used to extend the experimental data set so that the rate of wave attenuation can be evaluated over a larger number of wave lengths.

4.1. SWASH performance for wave transformation without mangroves

The SWASH model can improve its frequency dispersion by increasing the number of vertical layers. However, increasing the number of layers also means that the model becomes more computational costly in terms of practical engineering. Usually, a vertical coarse resolution (1–3 layers) is sufficient to describe the wave physics outside the surf zone (Van den Berg et al., 2015). In this study, a two layer model was chosen because it provides better prediction for wave transformation processes. Fig. 7 compares the root mean square wave height and the mean water level between the physical and numerical model with a different number of vertical layers in both regular and irregular cases.
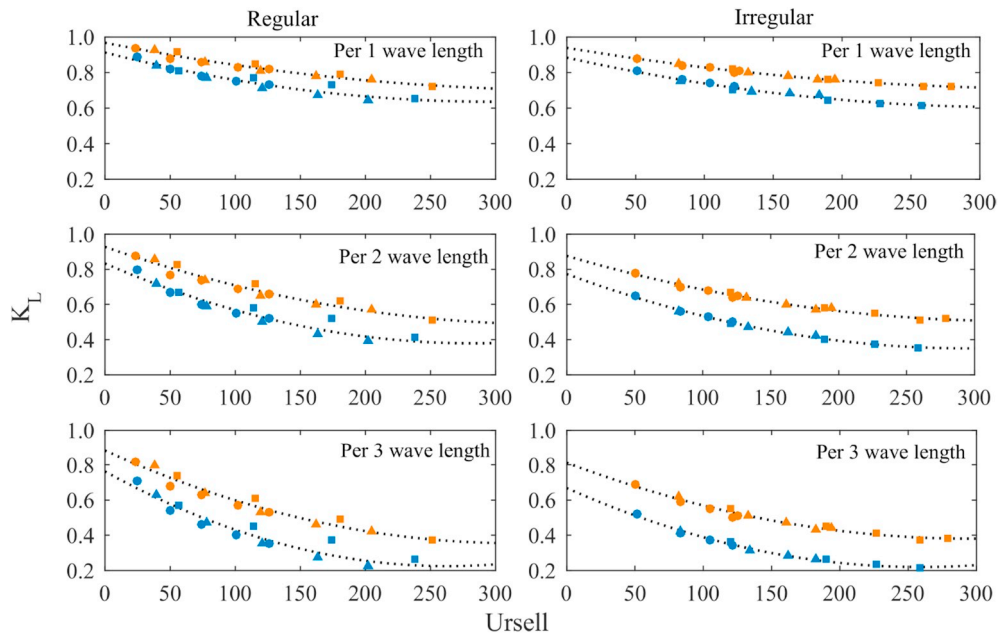
Fig. 6. Relationship between the effective transmission coefficient K_L and Ursell number for different wave height and periods: $T_p = 2$ s (circles), $T_p = 2.5$ s (triangles), $T_p = 3$ s (squares), different mangrove densities: sparse (orange), dense (blue) per one wave length (upper panels), per two wave lengths (middle panels), per three wave lengths (upper panels). The trend lines (dot lines) are second order polynomial lines. (For interpretation of the references to colour in this figure legend, the reader is referred to the Web version of this article.)

The predictive skill for different numbers of layers is presented in Table 2. The results suggest that the SWASH model with 2 or 3 vertical layers provide better agreement with the physical model than with 1 layer.

Increasing the number of layers from 1 to 2 layers significantly improves the predictive skill for the wave set up, especially in cases with irregular waves (the SI of the wave set up for 1 layer and 2 layer are 0.62 and 0.41, respectively). Moreover, increasing the number of layers from 2 to 3 layers does not substantially improve the predictive skill of the model. For example, the scatter index of *Hrms* for two and three layers in cases with regular waves are 0.09 and 0.07 and in cases with irregular waves are 0.12 and 0.11, respectively. Based on these

Table 2
Swash model skill for different number of vertical layers.

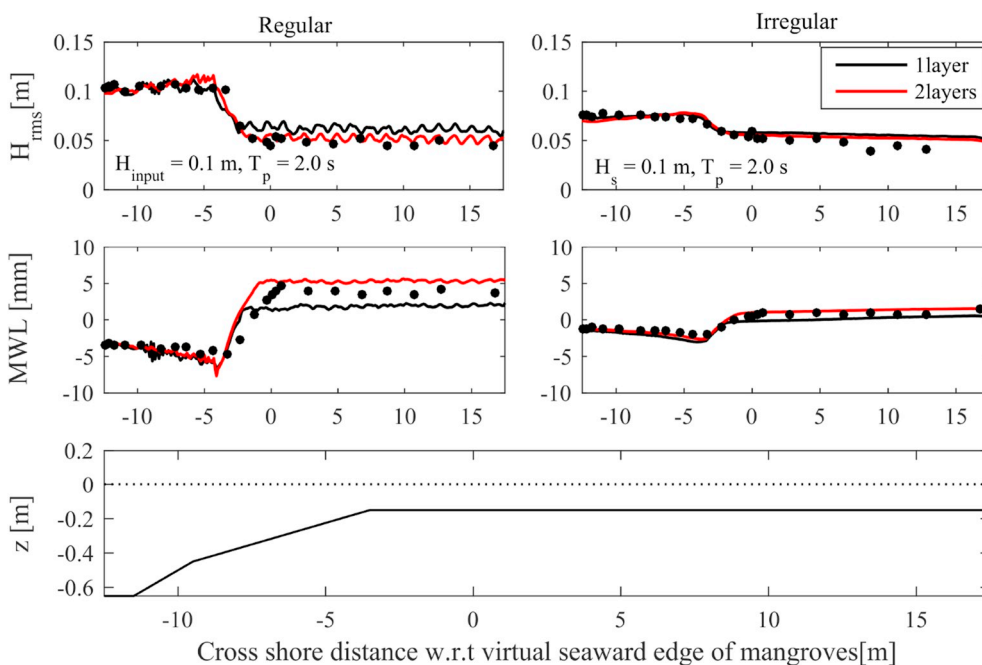| Case	ReH10T20			IrH10T20		
	1 layer	2 layers	3 layers	1 layer	2 layers	3 layers
BIAS Hrms [mm]	5.4	1.8	0.4	4.4	2.7	1.1
SI Hrms	0.15	0.09	0.07	0.14	0.12	0.11
BIAS set up [mm]	−0.1	−0.008	−0.008	−0.5	0.08	0.16
SI set up	0.44	0.43	0.43	0.62	0.41	0.46

Fig. 7. Comparisons between numerical model with 1 vertical layer (black line) and numerical model with 2 vertical layers (red line) and physical model (markers) for both regular (left hand side) and irregular wave (right hand side). (For interpretation of the references to colour in this figure legend, the reader is referred to the Web version of this article.)
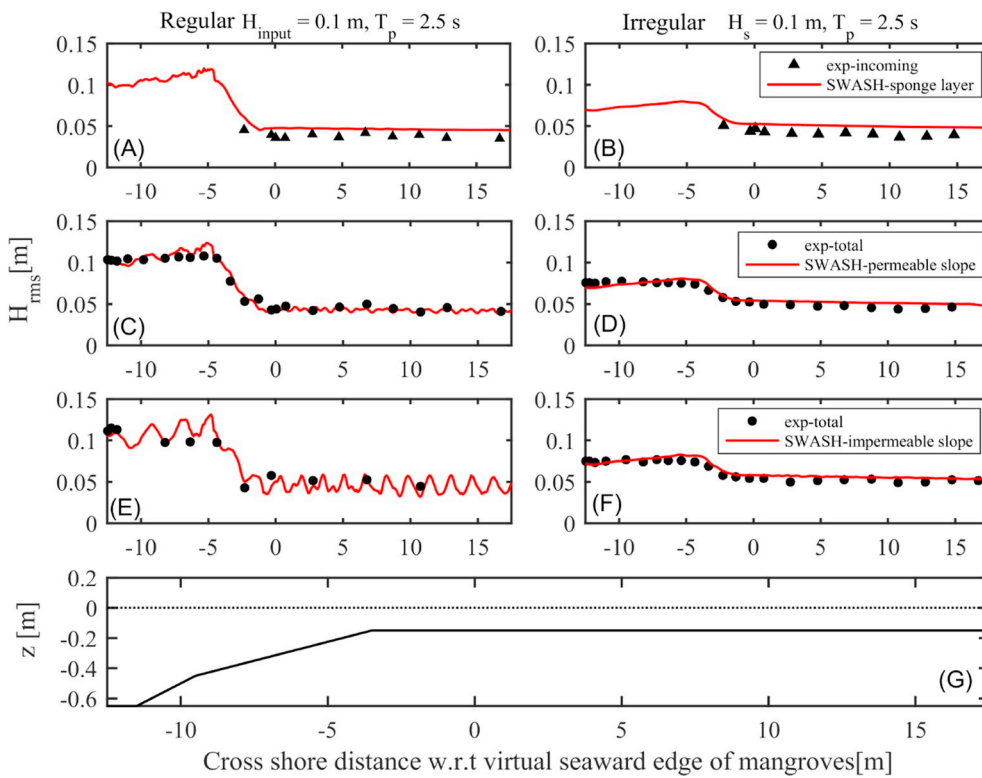
Fig. 8. Broken wave. Wave height comparisons between numerical model (red line) and physical model (markers) for 2 wave conditions ReH10T25 (left hand side) and IrH10T25 (right hand side) for 3 boundaries cases in SWASH. (For interpretation of the references to colour in this figure legend, the reader is referred to the Web version of this article.)

results, a two layer model was considered sufficient for this study.

As mentioned in the previous section, different boundary conditions at the end of the model can be imposed into the SWASH model. They include a sponge layer, a permeable slope and an impermeable slope. These options are sufficient to mimic the wave absorber and sea dike, which were considered in the physical model.

The upper panels (Fig. 8A and B) show the incoming wave height separated from the physical model and the associated results extracted from the numerical model with sponge layer. It can be seen that the wave height is slightly overestimated by the numerical model. The BIAS and Scatter index in cases with regular and irregular waves are 9.3 mm, 0.25 and 9.3 mm, 0.23 respectively. Because there is no wave reflection in the numerical model with a sponge layer, in order to compare the physical model with the numerical model the wave signal measured from the physical model was firstly separated incoming and reflected waves using Guza method (Guza et al., 1985). It is shown that this method can be used to separate the incoming and reflected waves in shallow water with an uncertainty of less than 10% (see Appendix A). This uncertainty may be the reason for a small difference in wave height between the physical and numerical model with the sponge layer. Although the simulation with sponge layer has larger BIAS and Scatter index than other cases (with wave absorbers and sea dikes), it is still in an acceptable range (less than 10%) and the SWASH model with sponge layer can be used to mimic scenarios without reflection waves.

The SWASH model with default values in cases with permeable and impermeable slopes can well reproduce the wave height transformation processes determined from the physical model (see 8C,D and Table 3).

For example, for regular and irregular cases with permeable slopes (wave absorber) there is only a small BIAS difference of 0.12 mm and 1.7 mm between physical model and numerical model, respectively. The scatter index numbers in those cases are also small (0.074 and 0.076 respectively).

Looking at the breaking processes (from $x = -5$ m to $x = 0$ m), it is noticed that in cases with regular waves (8C,E), the numerical model can well capture the breaking processes. However, in cases with irregular waves (8D,F) the waves appear to start breaking later than in the physical model. If only a few vertical layers (one to three layers) are implemented in SWASH, the amount of wave energy dissipation due to wave breaking may be underestimated, which can be compensated using a breaking command (Van den Berg et al., 2015). This command allows to initiate the wave breaking through a threshold parameter α and stop wave breaking through a threshold parameter β. In this study, α was varied in a range from 0.6 (default value) to 0.2 to get a better prediction of the breaking processes for irregular waves. It is shown that the predictive skill of SWASH can be improved by reducing α from 0.6 to 0.4 (BIAS reduce from 1.8 mm to 1 mm and SI reduce from 0.09 to 0.06 in case of wave absorber in the end) (see Table 4). Similar results can be observed in cases with a sea dike at the end of the flume (Table 4). Hence, the simulation of the breaking processes in cases with irregular waves can be improved by tuning the breaking parameter α in the breaking command. However, it is not really necessary because the difference is not significant (3% improvement). In conclusion, the above results confirm that the SWASH model using only default values can well reproduce the wave transformation and set up in the scenarios

Table 3
Statistic measures computed for wave height in case of different boundaries conditions.

Case	ReH10T25			IrH10T25		
	Sponge	Permeable	Impermeable	Sponge	Permeable	Impermeable
BIAS Hrms [mm]	9.4	0.12	−2	9.3	1.7	3.1
SI Hrms	0.25	0.074	0.1	0.22	0.076	0.068

Table 4
Statistic measures computed for wave height in case of different broken parameter alpha for irregular wave IrH10T20.

Case	Wave absorber			
	$\alpha = 0.6$	$\alpha = 0.4$	$\alpha = 0.3$	$\alpha = 0.2$
BIAS Hrms [mm]	1.8	1	−1.9	−0.7
SI Hrms	0.09	0.06	0.07	0.15
Case	Slope in the end			
BIAS Hrms [mm]	3.1	1.3	−2.1	−7.8
SI Hrms	0.075	0.055	0.08	0.16

without vegetation.

4.2. SWASH performance for wave transformation with mangroves

It is difficult to choose an appropriate bulk drag coefficient (C_d) to calculate the wave attenuation by vegetation due to the complexity of turbulence structures in and around the vegetation. Theoretically, in cases with rigid cylinder arrays and irrotational flow, $C_d = 1$.

In this part, the sensitivity of the SWASH model to the drag coefficient was studied. The drag coefficient (Cd) is an important parameter to characterize the flow and wave resistance due to the vegetation. In the literature, a relation between Cd and Reynolds number (Re) is usually suggested (see e.g. Suzuki et al. (2012)). Furthermore, relations between Cd and the Keulegan-Carpenter number (KC number) have also been suggested (Mendez and Losada, 2004; Augustin et al., 2009)).

Theoretically, a good estimation for forces on the cylinders can be achieved with an average value of the drag coefficient Cd equal to 1 combined with the local velocity. In reality however, the near-field flow pattern may affect the behavior of propagating oscillatory waves resulting in a fluctuation of Cd. As a result, the average value of Cd commonly is found to increase. Five different irregular cases and five different regular cases with two mangroves densities from the physical model were simulated with different values of C_d (from 1 to 1.6 with an interval of 0.2). It is suggested that the root-mean squared wave height measured in the experiment for both regular and irregular waves can be well reproduced in the simulations in sparse and dense cases with a bulk drag coefficient of 1.6 and 1.4, respectively (Fig. 9). It is noted that the 1D SWASH model does not account for the energy dissipation caused by turbulence processes in and around vegetation. In this sense, the increase in the magnitude of the C_d value can be interpreted to compensate for this missing mechanism of energy dissipation. In this study, the variation of Cd in the current laboratory experiment is expected to be small as the Reynolds number ranges from 1000 to 5000 and the KC number ranges from 15 to 150 ((Hu et al., 2014; Yan, 2014)). Therefore, in this study, an average drag coefficient of 1.5 was adopted for all considered simulation scenarios.

Fig. 10 illustrates the wave height transformation processes measured in the physical model and the associated results determined by the SWASH model with different densities of vegetation (no, sparse and dense mangrove). The results suggest that the wave height attenuation by cylinder arrays can be well predicted by the SWASH model (Fig. 10A,B,E,F,I,J). Although the wave height continues to reduce inside the vegetation, it can be clearly seen that there is a wave set-down
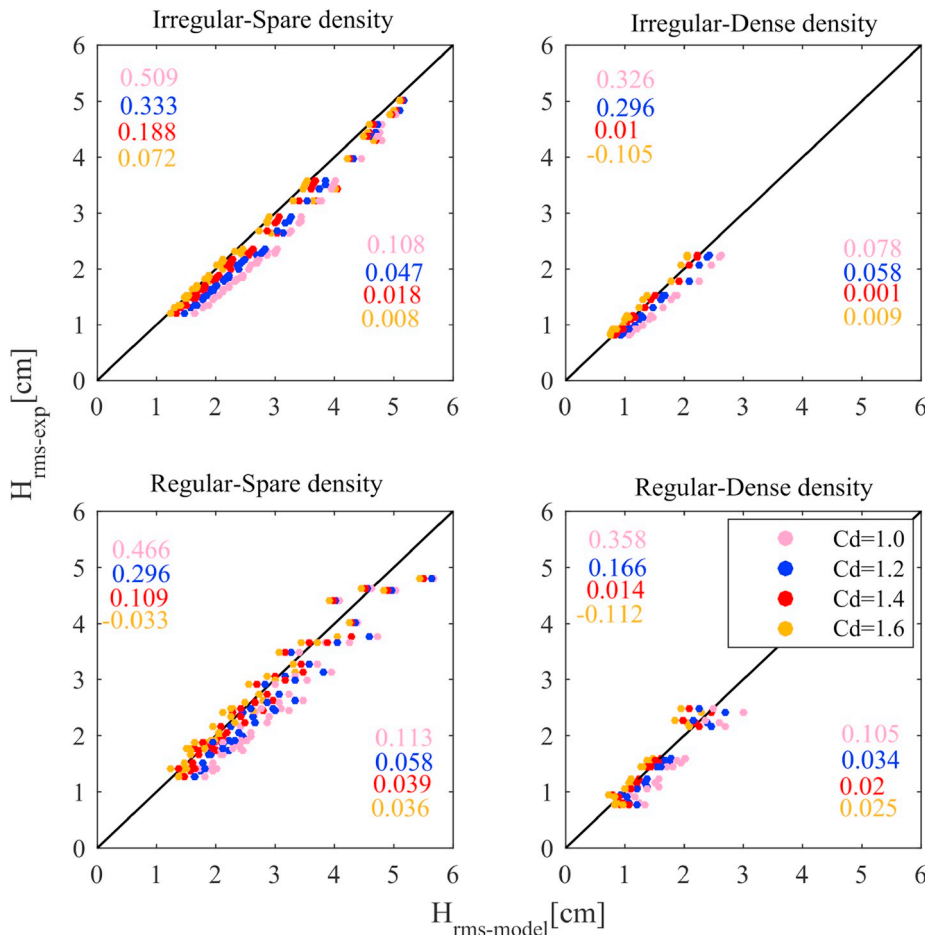

Fig. 9. Comparison of physical model (vertical) and numerical model (horizontal) root mean square wave height for irregular (A,B) and regular wave (C,D) in case of different mangroves densities: sparse density (A,C) and dense density (B,D). Four different values of the drag coefficient are used. The predicting skill of the model is represented by the bias (top left) and scatter index (bottom right) in each plot.
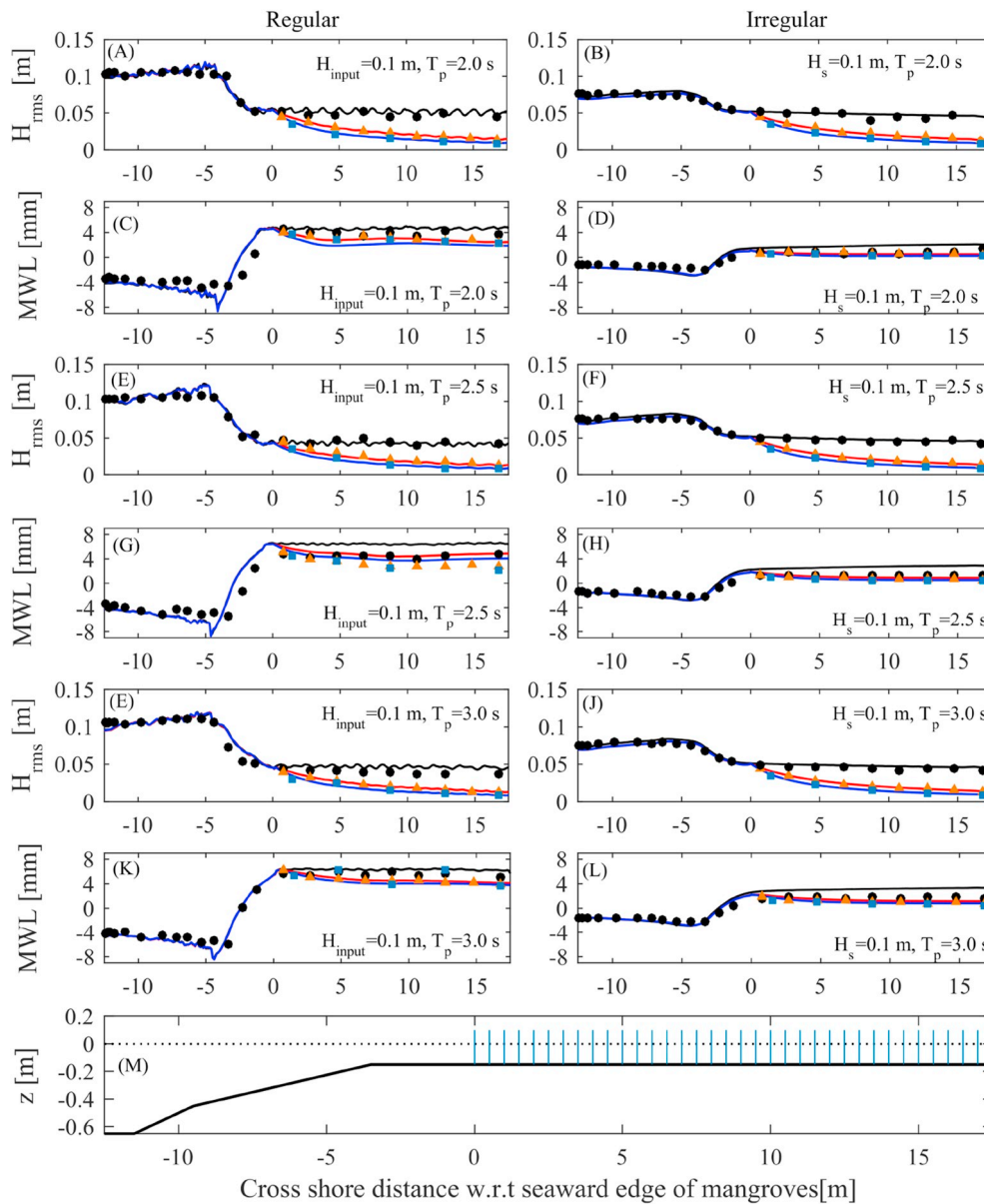
Fig. 10. Wave height transformation comparisons between physical model: without mangroves (black circles), sparse mangroves (orange triangles), dense mangroves (square blues) and numerical model: without mangroves (black line), sparse mangroves (red line), dense mangroves (blue line) for different wave height conditions. Regular waves are represented in the left hand side and irregular waves are represented in the right hand side. (For interpretation of the references to colour in this figure legend, the reader is referred to the Web version of this article.)

instead of set-up in the case of both regular and irregular waves. The balance of momentum flux and the drag force induced by the presence of cylinder arrays is the main reason of this phenomenon (Dean and Bender, 2006). It is noticed that in all cases, this phenomenon of wave set-down in stead of set-up inside the mangrove forest is also well reproduced by the numerical model (Fig. 10C,D,G,H,K,L).

4.3. Experimental data extended using the numerical model

In this section, the numerical model was used to extend the length of mangroves in the experiment from 17.5 m to 40 m (from five wave lengths to ten wave lengths). The wave conditions (wave height and wave periods) were taken the same as in the experiment. Representative cases with sparse vegetation and irregular waves with a wave absorber in the end was considered.

Fig. 11 shows the final extended results of wave attenuation determined for the effective transmission coefficient (K_L). The first part

(first five wave lengths) includes the original experimental results (red markers) and that determined by the model (black markers). It can be clearly seen that the model can well predict the wave attenuation for the first five wave lengths. Therefore, the extended part (next five wave lengths) is expected to be trustworthy. According to the numerical simulation, it is predicted that the rate of wave attenuation rate appears to be constant after about eight wave lengths where the changes in the wave attenuation rate become less than 5% in all cases for different Ursell numbers.

In this sense, the rate of wave attenuation by vegetation can be understood as a function of the number of wave lengths and Ursell numbers which can be generalized in an exponential equation:

$$K_L = ae^{bn} + ce^{dn} \qquad (7)$$

where n is the number of wave lengths and a, b, c, d are proportionality coefficients depending on the Ursell number. The relationship between these four coefficients and the Ursell numbers is presented in Fig. 12. In
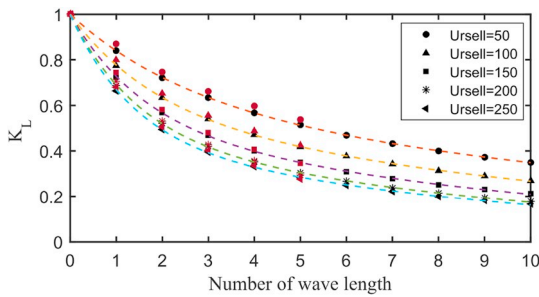
Fig. 11. Comparision the effective wave transmission K_L determined from physical model (red markers) and predicted from the numerical model (black markers). In cases of irregular waves, sparse vegetation with different Ursell numbers. Ursell = 50 (circles), Ursell = 100 (triangles), Ursell = 150 (squares), Ursell = 200 (stars), Ursell = 250 (left-pointing triangles). (For interpretation of the references to colour in this figure legend, the reader is referred to the Web version of this article.)
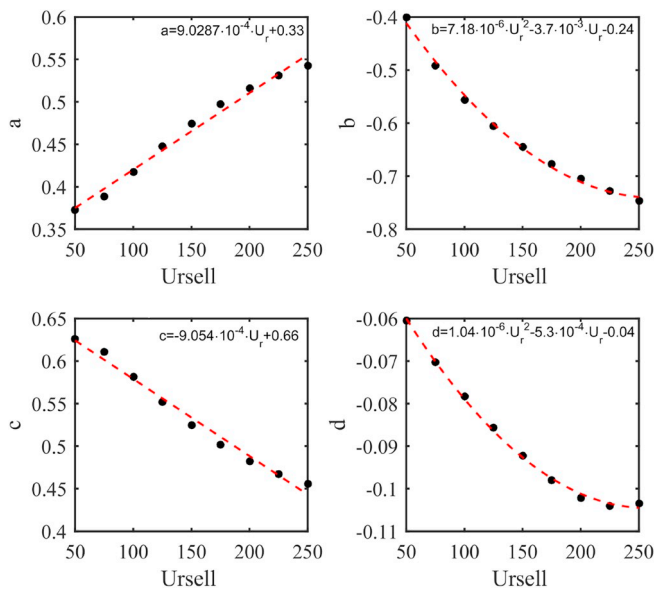

Fig. 12. Relationship between parameters a,b,c,d from Equation (7) and Ursell number.

this way, the wave height attenuation rate per number of wave length for a specific mangrove density can be presented as a function of the wave non-linearity presented by the Ursell number.

5. Conclusions

In this study, the wave attenuation process due to rigid vegetation was investigated, particularly focusing on the effect of wave non-linearity on the attenuation processes. Although many studies have been published on this topic, it is unclear how and to what extent the wave

characteristics affect this phenomenon. As a result, the attenuation rate of wave height in the literature is commonly presented and evaluated as a function of an arbitrary absolute length.

In order to obtain more insight, an experiment was performed with different scenarios covering a large range of wave characteristics, including regular, irregular, broken, and non-broken waves with different wave heights and wave periods. The results confirm the role of vegetation in attenuating the wave height. Moreover, a wave set-down instead of wave set-up due to the effect of vegetation was also observed.

The experimental data were used to evaluate the effects of the wave-non linearity on the wave reduction processes. An effective wave transmission coefficient is proposed, in which the wave height reduction is evaluated according to a relative length, i.e the number of wave lengths. Moreover, the wave characteristics are assessed through the Ursell number. It is shown that as the Ursell number increases from 0 to 250, the wave attenuation processes are also significantly affected. It is found that, the stronger the wave non-linearity, the stronger the attenuation of the wave height. For Ursell larger than 250, the wave attenuation processes appear to be independent of the wave characteristics. In this sense, if the characteristics of wave height (represented by Ursell) and vegetation (density, drag coefficient) are known, the attenuation rate of the waves can be derived.

Furthermore, a numerical model mimicking the physical model was constructed with the SWASH model. The numerical model then was validated using the experimental data. It is suggested that the model with only default values can well capture the transformation processes of the wave heights observed and measured in the physical model. A drag coefficient of 1.5 for all experiments is adopted to account for the turbulent energy dissipation processes that can not resolved in the simulations. Finally, the numerical model was used to extend the attenuation distance of the mangroves in the experiment so that the wave attenuation rate over up to ten wave lengths could be assessed. Based on that, the wave attenuation rate for a specific mangrove density can be presented as a function of the number of wave lengths and the Ursell number.

It is also noted that in SWASH, it is possible to prescribe different layers of vegetation, i.e. with different densities and stem sizes. This means that mangroves including their roots, stems and canopies can be included in the model. However, SWASH can only consider straight, vertical cylinders. The complexity of the tangled roots of mangroves cannot be described. Furthermore, flexible vegetation or in other words the motion of plants still cannot be imposed into the model. Moreover, the associated turbulence processes in and around vegetation are not considered in the model. Consequently, increasing the value of the drag coefficient Cd is usually chosen as a solution for this shortcoming.

Appendix A. Supplementary data

Supplementary data to this article can be found online at https://doi.org/10.1016/j.coastaleng.2019.01.004.

Appendix A

The methodology of Guza et al. (1985) was used to separate incoming and reflected wave for irregular and regular wave in cases without mangroves. This method is based on surface time series signal and velocity time series signal collected at the same locations. Wave conditions were performed for two different boundaries conditions *i.e.* with the wave absorber or with the sea dike at the end. The incoming wave signal determined in these both cases are the same indicating the accuracy of the method (see Fig. 13).
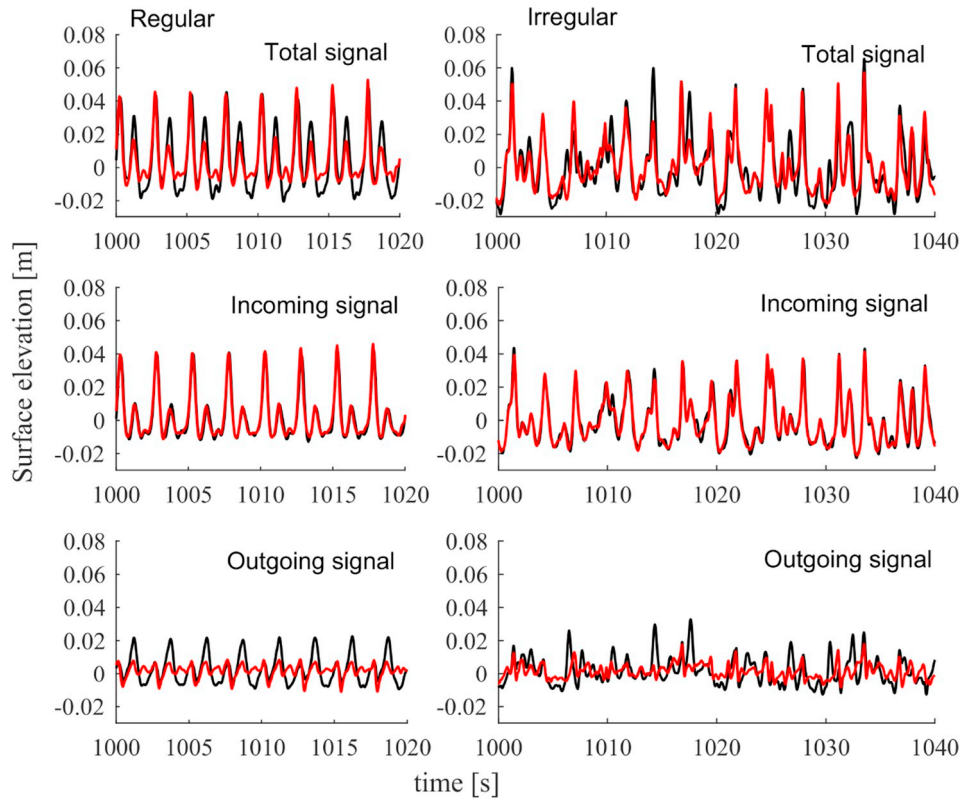
Fig. 13. Comparisons time series signal in case of sea dike in the end (black line) and wave absorber in the end (red line) for regular wave (left hand side) and irregular wave (right hand side) at x = 2.75[m] from the virtual seaward edge of the mangroves. Upper panels show total time series signal. Middle panels and lower panels showing incoming and outgoing time series signal separated by Guza method respectively. Wave condition: H = 10 cm; T = 2.5s..
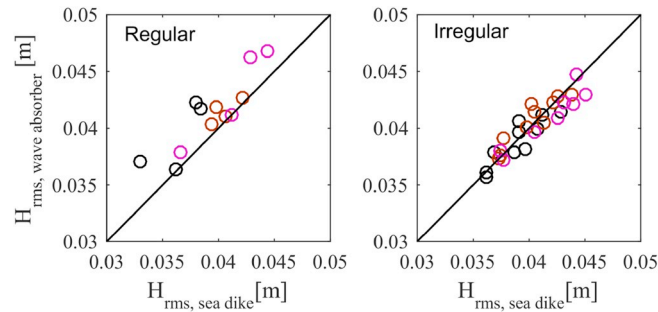

Fig. 14. Comparisons between incoming wave height in case of wave absorber in the end (vertical) and in case of sea dike in the end (horizontal) for irregular and regular wave..

The incoming wave heights determined by Guza's method for different wave conditions (H = 10 cm; T = 2s; 2.5s and 3s) in cases with wave absorber at the end were compared with that in cases with sea dikes at the end (Fig. 14). It is shown that this separation method achieves more than 90% accuracy.
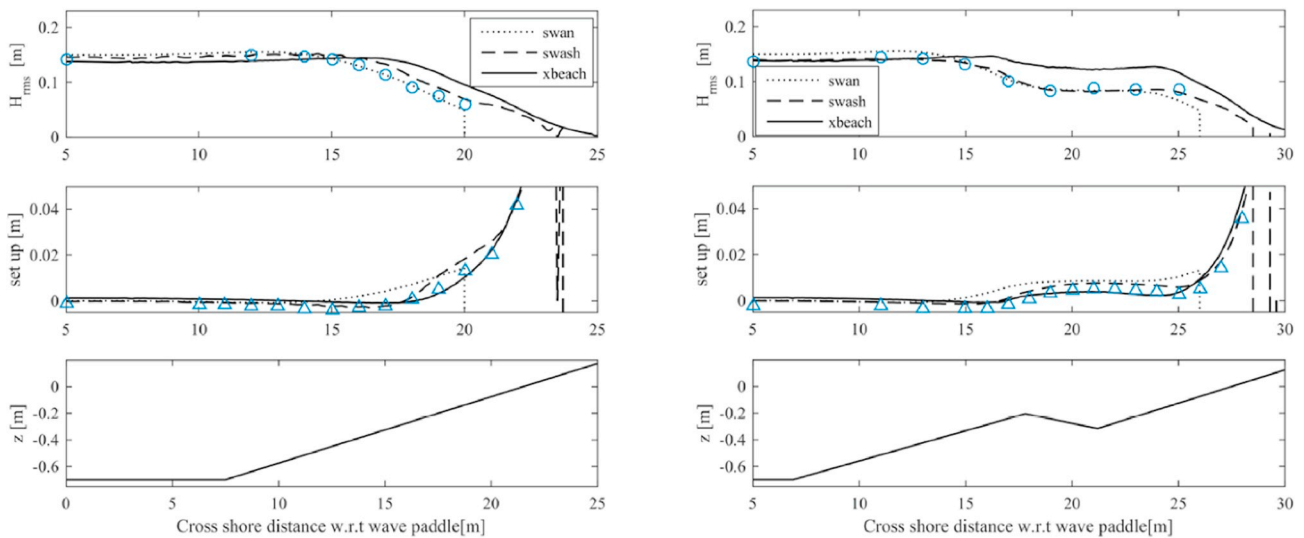
Appendix B

Fig. 15. An example of a comparison between, Swan, Xbeach and Swash simulation results using Battjes and Janssen (1978) experimental data set.

The modelling capability of three different wave models i.e. Swan, Xbeach and Swash was tested using the experimental data set of Battjes and Janssen (1978). The simulation results of these models are shown in figure. In all aspects the Swash model shows the best performance. Moreover, it is noted that the Swan model cannot include long waves and short waves. Based on the performance for these two nearshore cases Swash was selected for this study.

References

Anderson, M., Smith, J., 2015. Wave attenuation by flexible, idealized salt marsh vegetation. Coast. Eng. 83, 82–92. http://www.sciencedirect.com/science/article/pii/S0378383913001609 https://doi.org/10.1016/j.coastaleng.2013.10.004.

Augustin, L.N., Irish, J.L., Lynett, P., 2009. Laboratory and numerical studies of wave damping by emergent and near-emergent wetland vegetation. Coast. Eng. 56, 332–340.

Bao, T.Q., 2011. Effect of mangrove forest structures on wave attenuation in coastal vietnam. Oceanologia 53, 807–818.

Battjes, J.A., Janssen, J., 1978. Energy loss and set-up due to breaking of random waves. In Coast. Eng. 1978, 569–587.

Van den Berg, F., Beltman, W., Adriaanse, P., de Jong, A., Te Roller, J., 2015. SWASH Manual 5.3: Users Guide Version 5. Technical Report Statutory Research Tasks Unit for Nature & the Environment (WOT Natuur & Milieu.

Bradley, K., Houser, C., 2009. Relative velocity of seagrass blades: implications for wave attenuation in low-energy environments. J. Geophys. Res.: Earth Surface 114.

Brinkman, R.M., 2006. Wave Attenuation in Mangrove Forests: an Investigation through Field and Theoretical Studies. Ph.D. thesis James Cook University.

Brinkman, R.M., Massel, S.R., Ridd, P.V., Furukawa, K., et al., 1997. Surface wave attenuation in mangrove forests. In: Pacific Coasts and Ports' 97: Proceedings of the 13th Australasian Coastal and Ocean Engineering Conference and the 6th Australasian Port and Harbour Conference Volume 2. Centre for Advanced Engineering, University of Canterbury, pp. 909.

Buckley, M., Lowe, R., Hansen, J., 2014. Evaluation of nearshore wave models in steep reef environments. Ocean Dynam. 64, 847–862.

Cao, H., Feng, W., Chen, Y., 2016. Numerical modeling of wave transformation and runup reduction by coastal vegetation of the south China sea. J. Coast Res. 75, 830–835.

Cavallaro, L., Re, C.L., Paratore, G., Viviano, A., Foti, E., 2011. Response of posidonia oceanica to wave motion in shallow-waters-preliminary experimental results. Coastal Engineering Proceedings 1, 49.

Cooper, N.J., 2005. Wave dissipation across intertidal surfaces in the wash tidal inlet, eastern england. J. Coast Res. 28–40.

Dalrymple, R.A., Kirby, J.T., Hwang, P.A., 1984. Wave diffraction due to areas of energy dissipation. J. Waterw. Port, Coast. Ocean Eng. 110, 67–79.

Dean, R.G., Bender, C.J., 2006. Static wave setup with emphasis on damping effects by vegetation and bottom friction. Coast. Eng. 53, 149–156.

Guza, R., Thornton, E., Holman, R., 1985. Swash on steep and shallow beaches. In Coast. Eng. 1984, 708–723.

Hu, Z., Suzuki, T., Zitman, T., Uittewaal, W., Stive, M., 2014. Laboratory study on wave dissipation by vegetation in combined current–wave flow. Coast. Eng. 88, 131–142.

Lövstedt, C.B., Larson, M., 2009. Wave damping in reed: field measurements and mathematical modeling. J. Hydraul. Eng. 136, 222–233.

Massel, S., 2006. Experiments on Wave Motion and Suspended Sediment Concentration at Nang Hai, Can Gio Mangrove Forest, Southern Vietnam. Oceanologia 48.

Mazda, Y., Magi, M., Ikeda, Y., Kurokawa, T., Asano, T., 2006. Wave reduction in a mangrove forest dominated by sonneratia sp. Wetl. Ecol. Manag. 14, 365–378.

Mazda, Y., Magi, M., Kogo, M., Hong, P.N., 1997. Mangroves as a coastal protection from waves in the tong king delta, vietnam. Mangroves Salt Marshes 1, 127–135.

Mendez, F.J., Losada, I.J., 2004. An empirical model to estimate the propagation of random breaking and nonbreaking waves over vegetation fields. Coast. Eng. 51, 103–118.

Möller, I., 2006. Quantifying saltmarsh vegetation and its effect on wave height dissipation: results from a UK east coast saltmarsh. Estuar. Coast Shelf Sci. 69, 337–351.

Möller, I., Spencer, T., 2002. Wave dissipation over macro-tidal saltmarshes: effects of marsh edge typology and vegetation change. J. Coast Res. 36, 506–521.

Möller, I., Spencer, T., French, J.R., Leggett, D., Dixon, M., 1999. Wave transformation over salt marshes: a field and numerical modelling study from north norfolk, england. Estuarine. Coastal and Shelf Science 49, 411–426.

Mork, M., 1996. Wave attenuation due to bottom vegetation. In: Waves and Nonlinear Processes in Hydrodynamics. Springer, pp. 371–382.

Phan, L.K., van Thiel de Vries, J.S., Stive, M.J.F., 2014. Coastal mangrove squeeze in the mekong delta. J. Coast Res. 31, 233–243.

Quartel, S., Kroon, A., Augustinus, P., Van Santen, P., Tri, N., 2007. Wave attenuation in coastal mangroves in the red river delta, vietnam. J. Asian Earth Sci. 29, 576–584.

Suzuki, T., Zijlema, M., Burger, B., Meijer, M.C., Narayan, S., 2012. Wave dissipation by vegetation with layer schematization in swan. Coast. Eng. 59, 64–71.

Wu, W.-C., Cox, D.T., 2015. Effects of wave steepness and relative water depth on wave attenuation by emergent vegetation. Estuar. Coast Shelf Sci. 164, 443–450.

Yan, N., 2014. Drag Forces on Vegetation Due to Waves and Currents. Master thesis. TU Delft.

Zijlema, M., 2012. Modelling wave transformation across a fringing reef using swash. Coastal Engineering Proceedings 1, 26.

Zijlema, M., Stelling, G., Smit, P., 2011a. Simulating nearshore wave transformation with non-hydrostatic wave-flow modelling. In: Conference Proceedings, 12th Int. Workshop on Wave Hindcasting and Forecasting, Hawaii, USA.

Zijlema, M., Stelling, G., Smit, P., 2011b. Swash: an operational public domain code for simulating wave fields and rapidly varied flows in coastal waters. Coast. Eng. 58, 992–1012.